Spatial and temporal changes of the ozone sensitivity in China based on satellite and ground-based observations

Wannan Wang[1,2,3], Ronald van der A[3], Jieying Ding[3], Michiel van Weele[3] and Tianhai Cheng[1]

[1]Aerospace Information Research Institute, Chinese Academy of Sciences, Beijing, 100094, China
[2]University of Chinese Academy of Sciences, Beijing, 100049, China
[3]Royal Netherlands Meteorological Institute (KNMI), De Bilt, 3730 AE, the Netherlands

Correspondence to: Ronald van der A (ronald.van.der.a@knmi.nl)

Abstract. Ground-level ozone (O_3) pollution has been steadily getting worse in most part of eastern China during the past five years. The non-linearity of O_3 formation with its precursors like nitrogen oxides (NO_x = NO + NO_2) and volatile organic compounds (VOCs) are complicating effective O_3 abatement plans. The diagnosis from space-based observations, the ratio of formaldehyde (HCHO) columns to tropospheric NO_2 columns (HCHO/NO_2), has previously been proved to be highly consistent with our current understanding of surface O_3 chemistry. HCHO/NO_2 ratio thresholds distinguishing O_3 formation sensitivity depend on regions and O_3 chemistry interactions with aerosol. To shed more light on current the O_3 formation sensitivity over China, we have derived HCHO/NO_2 ratio thresholds by directly connecting satellite-based HCHO/NO_2 observations and ground-based O_3 measurements over the major Chinese cities in this study. We find that a VOC-limited regime occurs for HCHO/NO_2 < 2.3 and NO_x-limited regime occurs for HCHO/NO_2 > 4.2. The HCHO/NO_2 between 2.3 and 4.2 reflects the transition between the two regimes. Our method shows that the O_3 formation sensitivity tends to be VOC-limited over urban areas and NO_x-limited over rural and remote areas in China. We find that there is a shift in some cities from the VOC-limited to the transitional regime that is associated with a rapid drop of anthropogenic NO_x emissions owing to the widely-applied rigorous emission control strategies between 2016 and 2019. This detected spatial expansion of the transitional regime is supported by rising surface O_3 concentrations. The enhanced O_3 concentrations in urban areas during the COVID-19 lockdown in China indicate that a protocol with simultaneous anthropogenic NO_x emissions and VOC emissions controls is essential for O_3 abatement plans.

1 Introduction

Ground-level ozone (O_3) is one of major air pollutants that has negative impacts on human health and can result in eye and nose irritation, respiratory disease, and lung function impairment (Jerrett et al., 2009; Khaniabadi et al., 2017; Huang et al., 2018). Tian et al. (2020b) observed increased admissions for pneumonia associated with O_3 exposure, especially for elderly people. In addition, it also has important impacts on climate as a greenhouse gas by absorbing thermal radiation (Fishman et al., 1979; IPCC, 2014). Photochemical tropospheric O_3 is formed in a nonlinear manner from O_3 precursors such as volatile organic compounds (VOCs) and nitrogen oxides (NO_x = NO + NO_2) in the presence of sunlight (Crutzen, 1974; Jacob, 2000).

In 2008, China was found to be the largest contributor to Asian emissions of carbon monoxide (CO), NO_x, non-methane volatile organic carbon (NMVOC), and methane (CH_4) (Kurokawa et al., 2013). Because of these large emissions of anthropogenic air pollutants, the Chinese State Council released the "Air Pollution Prevention and Action Plan" (APPAP) on September 2013, which has as a key task to prevent and control air pollution in China (Cai et al., 2017). Since then, critical emission control strategies have been carried out that are designed to reduce the concentrations of six environmental pollutants: sulfur dioxide (SO_2), nitrogen dioxide (NO_2), CO, O_3, and particulate matter ($PM_{2.5}$ and PM_{10}) (Zhang et al., 2016; Feng and Liao, 2016). During the past decade, the concentrations of many pollutants including SO_2, NO_2, CO, $PM_{2.5}$ and PM_{10} have declined in most cities, however, O_3 concentrations showed an increasing trend (Wang et al., 2017b; Wang et al., 2019b; Zeng et al., 2019). Therefore, reducing O_3 concentrations has become the focus of China's next air quality control strategies (Cheng et al., 2018).

In terms of O_3 concentrations, the effectiveness of emissions control strategy depends on whether the photochemical regime of O_3 formation is VOC-limited or NO_x-limited (Jin et al., 2020). In the VOC-limited (or NO_x-saturated) regime, VOC emission reductions reduce the chemical production of organic radicals (RO_2), which in turn lead to decreased cycling with NO_x and consequently lower concentration of O_3 (Milford et al., 1989). In NO_x-limited (or VOC-saturated) regime, NO_x emission reductions reduce NO_2 photolysis, which is the primary source of free oxygen atoms. Therefore, in a NO_x-limited regime, NO_x reductions reduce ambient O_3. In contrast, in VOC-limited regime, NO_x acts to reduce O_3, so a NO_x decrease in emissions promotes O_3 production (Kleinman, 1994).

The observed photochemical indicators and observation-based models (OBM) are the most commonly used tools to diagnose the O_3 formation sensitivity. O_3 production efficiency (OPE=$\Delta O_3/\Delta NO_z$) and the H_2O_2/NO_z (or H_2O_2/HNO_3) ratio are two widely used indicators to infer the O_3 formation regimes (Chou et al., 2011; Ding et al., 2013). Wang et al. (2017a) concluded that lower OPE values (e.g., < 4) indicate a VOC-limited regime. In contrast, higher OPE values (e.g., >7) indicate a NO_x-limited regime. OPE values in the medium range (e.g., 4 < OPE < 7) mark the transition between two regimes. Another indicator of the O_3 formation sensitivity regime is the H_2O_2/NO_z ratio. Hammer et al. (2002) defined that in the VOC-limited regime, lower H_2O_2/NO_z ratios would be expected and higher H_2O_2/NO_z ratios indicate the NO_x-limited regime. In the past decade, the observed photochemical indicators have been applied to identify the O_3 formation sensitivity in different periods and regions of China.

The OBM combines *in-situ* field observations and chemical box modeling. It is built on widely-used chemistry mechanisms (e.g., MCM, Carbon Bond, RACM or SAPRC), and applied to the observed atmospheric conditions to simulate various atmospheric chemical processes, including the *in-situ* O_3 production rate. However, ground-based measurements are often limited in time period and spatial extent. The OBM analysis requires measuring nitric oxide (NO) at sub-ppb levels and more than 50 different types of VOCs and with high accuracy, which is difficult to achieve (Wang et al., 2017a).

Satellite remote sensing provides an alternative way to investigate long time periods of O_3 formation sensitivity on large spatial scales. For over two decades, satellite-based spectrometers have provided continuous global observations on a daily basis for two species indicative of O_3 precursors, NO_2 for NO_x (Martin et al., 2004; Lamsal et al., 2014) and formaldehyde

(HCHO) for VOC (Palmer et al., 2003; Fu et al., 2007). NO_x can be approximated from satellite observation of NO_2 column because of the short lifetime of NO_x and high ratio of NO_2/NO_x in the boundary layer (Duncan et al., 2010; Jin and Holloway, 2015). HCHO is an intermediate of the oxidation reaction of various VOCs in the atmosphere. The production of HCHO is approximately proportional to the summed rate of reactions of VOC with OH radicals (Sillman, 1995). Therefore, HCHO can be used as a tracer for VOCs in the absence of other VOC observations (Martin et al., 2004; Duncan et al., 2010). The O_3 formation sensitivity is defined by the ratio of HCHO to NO_2 (referred to as FNR) (Martin et al., 2004). Duncan et al. (2010) combined models and OMI HCHO and NO_2 data to show certain ranges of FNR that can be useful for classifying a region into VOC-limited or NO_x-limited regime. A FNR smaller than 1 indicates the VOC-limited conditions, and a FNR higher than 2 to indicate the NO_x-limited conditions. A FNR in the range of 1 - 2 should generally be considered as indicative of the transitional regime. These FNR thresholds defined by Duncan et al. (2010) have been widely used for various regions (Choi and Souri, 2015; Jin and Holloway, 2015; Souri et al., 2017; Jeon et al., 2018) and with different satellite instruments (Choi et al., 2012).

However, these prior studies linked FNR with surface O_3 sensitivity in models (Martin et al., 2004; Duncan et al., 2010). Modeled and observed HCHO columns, NO_2 columns and surface O_3 often disagree. Jin et al. (2017) found that the spatial and temporal correlations between the modeled and satellite-derived FNR vary over the used satellite instruments. Brown-Steiner et al. (2015) found persistent O_3 biases under all configurations of the Global Climate-Chemistry Model (GCCM) with detailed tropospheric chemistry. Although FNR thresholds defined by Duncan et al. (2010) have been used previously to investigate O_3-NO_x-VOC sensitivity in China (Witte et al., 2011; Tang et al., 2012; Jin and Holloway, 2015), their conclusions were based on the atmospheric situations in the United States and may not be suitable for the more complicated air pollution in China, concerning the different emission factors, sources, pollution levels and climatology. For example, compared with United States, most cities in China have higher aerosol levels (van Donkelaar et al., 2010; Li et al., 2019c). Secondary aerosol production may become a large sink of radicals, which could shift O_3 production toward a VOC-limited regime under these FNR thresholds suited to United States (Liu et al., 2012; Li et al., 2019a). It is therefore useful to describe surface O_3 sensitivity using FNR thresholds derived entirely from satellite observed FNR and ground-based measurements of O_3. In addition, Schroeder et al. (2017) using airborne measurements suggested that the range and span of FNR marking the transitional regime varies regionally.

In this study, we assess if space-based $HCHO/NO_2$ ratio captures the non-linearity of O_3 chemistry by matching satellite observations with ground-based O_3 measurements over the major Chinese cities. Thresholds suited for China between space-based $HCHO/NO_2$ and the ground-based O_3 response patterns are derived from observations instead of model results. We focus on the spatial and temporal variability of O_3 formation sensitivity using our FNR thresholds on a nationwide scale and in typical cities from 2016 to 2019.

More recently a new unique situation has occurred with the outbreak of the COVID-19 pandemic, which provided a unique opportunity to demonstrate our predicted effects on O_3 pollution in China. Efforts to halt the spread of COVID-19 have drastically reduced human activities worldwide (Siciliano et al., 2020; Tian et al., 2020a). As a result of these restrictions, a significant reduction in primary air pollutant emissions, especially in the concentration of NO_2, has been noticed in China and

several European and American countries (Tobías et al., 2020; Wang and Su, 2020; Bauwens et al., 2020; Ding et al., 2020). By contrast, increasing O_3 concentrations during the same period were observed in densely metropolitan areas throughout the world (Siciliano et al., 2020; Zoran et al., 2020; Huang et al., 2020).

Section 2 describes the data and methods used in this study. Section 3 presents our derived FNR thresholds method and variations of O_3 formation sensitivity in China. In addition, impacts of the COVID-19 outbreak on O_3 levels are discussed. Finally, section 4 gives a brief summary.

2 Data

2.1 Satellite data

We use the NO_2 and HCHO observations from the Ozone Monitoring Instrument (OMI) aboard the National Aeronautics and Space Administration (NASA) satellite AURA, which was launched in July 2004 (Levelt et al., 2006). In an ascending sun-synchronous polar orbit, OMI passes the equator at about 13:40 local time (LT), providing global measurements of aerosol parameters, cloud, and various trace gases (NO_2 and HCHO among them) (Levelt et al., 2006). The high spatial resolution (13 km × 24 km at nadir) allows for observing fine details of atmospheric parameters (Jin and Holloway, 2015). OMI data are considered to be reliable and of good quality for the full mission thus far (Zara et al., 2018). In addition, the OMI overpass time is well suited to detect the O_3 formation sensitivity during the afternoon, when O_3 photochemical production peaks and when the boundary layer is high and the solar zenith angle is small, maximizing instrument sensitivity to HCHO and NO_2 in the lower troposphere (Jin et al., 2017).

We use the OMI tropospheric NO_2 and HCHO data products from the European Quality Assurance for Essential Climate Variables project (QA4ECV, http://www.qa4ecv.eu/). NO_2 data are compiled by the Royal Netherlands Meteorological Institute (KNMI). The tropospheric NO_2 column density, is defined as the vertically integrated number of NO_2 molecules between the Earth's surface and the tropopause per unit area. We select QA4ECV NO_2 daily observations following the recommendations given in the Product Specification Document (Boersma et al., 2011) for this data product: (1) no processing error; (2) less than 10% snow or ice coverage; (3) solar zenith angle less than 80˚; (4) cloud radiance fraction less than 50%. The QA4ECV NO_2 monthly datasets are processed with a spatial resolution of $0.125° \times 0.125°$. Boersma et al. (2018) reported the single-pixel uncertainties for the QA4ECV NO_2 columns are 35% - 45% in the polluted regions, the monthly mean NO_2 columns are estimated to have an uncertainty of ±10%.

The OMI tropospheric HCHO are retrieved by the Belgian Institute for Space Aeronomy (BIRA-IASB) (Smedt et al., 2017). We select processing_quality_flags = 0 or > 255 providing a selection of observations that is considered as optimal. Zara et al. (2018) found that the QA4ECV HCHO slant column densities (SCDs) have uncertainties of 8 - 12 × 10^{15} molecule/cm^2 and a remarkably stable trend (increase < 1% $year^{-1}$). The QA4ECV HCHO monthly datasets are available with a spatial resolution of $0.05° \times 0.05°$. Temporal averaging has been shown to reduce the HCHO measurements uncertainty and

noise (Millet et al., 2008). We re-grid the monthly OMI HCHO data ($0.05° \times 0.05°$) to the same grid as for the monthly OMI NO_2 data ($0.125° \times 0.125°$).

2.2 NO_x emission

Emission inventories of air pollutants are important sources of information for policy makers and form essential input for air quality models. Bottom-up inventories are usually compiled from statistics on emitting activities and their typical emission factors, but are sporadically updated (Li et al., 2017). Satellite-derived emission inventories have important advantages over bottom-up emission inventories: they are spatially consistent, have high temporal resolution, and provide up-to-date emission information (Mijling and van der A, 2012). In this study, we use monthly mean NO_x surface emission estimates derived from OMI observations of tropospheric NO_2 columns (the QA4ECV product discussed in section 2) by the Daily Emission estimation Constrained by Satellite Observations (DECSO) algorithm. Mijling and van der A (2012) for the first time developed DECSO (version 1) by calculating the sensitivity of concentration to emission based on a chemical transport model and using trajectory analysis to account for transport away from the source. Ding et al. (2015) improved DECSO (version 3) and demonstrated that it is able to detect the monthly change of NO_x emissions due to air quality regulations on a city level. The NO_x emissions derived by the improved DECSO version 5 are in good agreement with other bottom-up anthropogenic emission inventories. In addition, the improved algorithm is able to better capture the seasonality of NO_x emissions. The precision of monthly NO_x emissions derived by DECSO version 5 for each grid cell is about 20 % (Ding et al., 2017). Here, we use NO_x emissions derived by the latest DECSO version 5.1qa which provides monthly emissions for the last decade (2007-2020) (Ding et al., 2018). These datasets are available from https://www.temis.nl/emissions/region_asia/datapage.php.

2.3 Ground-based observations

Since 2012 the Chinese government at various levels began to establish a national air quality monitoring network, which released real-time ground-level O_3 monitoring data to the public. By 2016, the establishment of more than 1,000 sites have been completed, covering more than 300 cities across the country. At each monitoring site, the concentration of O_3 is measured using the ultraviolet absorption spectrometry method and differential optical absorption spectroscopy, NO_2 is measured using the chemi-luminescence method by a set of commercial instruments. The instrumental operation, maintenance, data assurance and quality control were conducted based on the most recent revisions of China Environmental Protection Standards (CMEE, 2013).

We use hourly O_3 and NO_2 concentrations (in standard condition, 273 K, 101.325 kPa) from the network of ~1000 sites operated by the China Ministry of Ecology and Environment (CMEE) since 2016. CMEE revised the monitoring of pollutants to a new reference condition (298K, 101.325 kPa) since 1 September 2018 (CMEE, 2018). Daily ground-based O_3 and NO_2 observations are calculated from hourly observations at OMI overpass time (average of 13:00 LT and 14:00 LT). In this study, we convert the gas concentrations before 1 September 2018 from the standard condition to the reference condition. The temperature dependence is according to Charles's law (1)

$$\frac{V_{std}}{T_{std}} = \frac{V_{ref}}{T_{ref}} \quad (1)$$

where V_{std} is the volume of a gas under standard condition, V_{ref} is the volume of a gas under reference condition, T_{std} (unit: K) is the thermodynamic temperature of standard condition, T_{ref} (unit: K) is the thermodynamic temperature of reference condition.

The gas concentration conversion follows

$$\frac{C_{std}}{C_{ref}} = \frac{M/V_{std}}{M/V_{ref}} = \frac{V_{ref}}{V_{std}} \quad (2)$$

where C_{std} is the gas concentration under standard condition, C_{ref} is the gas concentration under reference condition.

Because the Chinese national air quality monitoring network stations are mostly located in the center of cities or densely populated areas, usually the most polluted regions, we select the NaHa station located on the small island Okinawa in Japan, as a location with a clean atmosphere. The hourly O_3 and NO_2 observations of NaHa station are provided by the Japanese Atmospheric Environmental Regional Observation System (AEROS, http://soramame.taiki.go.jp/Index.php).

2.4 CLASS model

We simulate the nonlinear relationship among O_3, NO_2 and HCHO using the Chemistry Land-surface Atmosphere Soil Slab model (CLASS). We performed a series of numerical experiments with the same dynamic and chemistry conditions listed in Table 1, but modified only the concentrations of NO_2 and HCHO. The initial mixing ratios of chemical species are shown in Table S1 in the supplement. The initial mixing ratios data are from van Stratum et al. (2012). All other species (except for molecular oxygen and nitrogen) are initialized at zero, and modified only the concentrations of NO_2 and HCHO.

The CLASS model solves the diurnal evolution of dynamical variables (temperature, specific humidity and wind) and chemical species over time in a well-mixed, convective Atmospheric Boundary Layer (ABL) in which entrainment and boundary layer growth are considered (Vilà-Guerau de Arellano et al., 2015; van Heerwaarden et al., 2010). All these variables are assumed to be constant with height due to intense turbulent mixing driven by convection (van Heerwaarden et al., 2010). The surface is assumed to be homogeneous in this box model. Chemistry is represented by a chemical scheme based on 27 reactions that control O_3 formation described by van Stratum et al. (2012), with O_3, NO_x and isoprene as most important species. This simplified chemical scheme is able to represent the evolution of chemical species in semirural areas (Janssen et al., 2012; van Stratum et al., 2012). This chemical scheme is able to represent the evolution of O_3-NO_x-VOC-HO_x cycle in semirural areas (Vil`a-Guerau de Arellano et al., 2011; Janssen et al., 2012; van Stratum et al., 2012). The model has been validated under various dynamical conditions (Barbaro et al., 2014; Janssen et al., 2012; van Heerwaarden et al., 2010).

Table 1. Configuration and settings of CLASS modeling system

Item	**Status/Values**
Total simulation time	12h
Time step	60s

Initial ABL height	200m
Mixed-layer	On
Initial mixed-layer potential temperature	288K
Initial temperature jump at height	1K
Wind	Off
Surface scheme (sea or land)	Off
Chemistry	On

3 Results

3.1 O_3 formation sensitivity regime classification

In Figure 1a, the CLASS model is applied to generate O_3 isopleths, which illustrate O_3 as function of NO_2 and HCHO values. The isopleths show that O_3 formation is a highly nonlinear process in relation to NO_2 and HCHO. When NO_2 is low, the O_3 increases with increasing NO_2. As NO_2 increases, the O_3 eventually reaches a local maximum. At higher NO_2 concentrations, the O_3 would decrease with increasing NO_2.

We first evaluate if satellite-based HCHO and NO_2 columns can capture the nonlinear O_3-NO_2-HCHO chemistry shown by the CLASS model. In order to obtain a representative observation sample, we create monthly mean ground-based O_3 and NO_2 observations of 360 cities across China from the Chinese national air quality monitoring network from 2016 to 2019, and the background station observations from NaHa, Japan for comparison. Temperature is also a major factor in O_3 chemistry. O_3 pollution is rare when the ambient temperature is below 20 ℃ (Sillman, 2003). The seasonality of ground-level O_3 concentrations also exhibited monthly variability peaking in summer and reaching the lowest levels in winter over China (Wang et al., 2017b). In addition, long NO_x lifetime and low concentrations of OH and RO_2 radicals would lead most regions of China to a VOC-limited regime in winter (Shah et al., 2020). Therefore, we focus in this study on May - October as the summer period when meteorology is favorable for O_3 formation (Jin et al., 2017).

By directly connecting HCHO columns from OMI observations with ground-based measurements of NO_2 and O_3 from 360 cities across China during May – October from 2016 to 2019 in Figure 1b, we find that the satellite-based HCHO columns and ground-based NO_2 concentrations can capture nonlinear O_3 chemistry consistent with the CLASS model results. It indicates that tropospheric HCHO columns from OMI can represent the near-surface HCHO environment as revealed by previous studies (Martin et al., 2004; Duncan et al., 2010; Jin et al., 2017). The overall O_3-NO_2-HCHO chemistry is also captured by satellite-based HCHO and NO_2 columns in Figure 1c, where we construct the O_3 isopleth using only observations.

Having established this relationship between satellite-based HCHO/NO_2 columns and surface O_3 concentrations, we subsequently derive the FNR thresholds marking the O_3 transitional regime. The local O_3 maximum can be thought of as a dividing line separating two different photochemical regimes (Sillman, 1999). According to the National Ambient Air Quality

Standards released in 2012, 1-hour average O_3 concentration should below 160 μg/m^3 in rural regions and below 200 μg/m^3 in urban regions (Li et al., 2018). We assume that the monthly O_3 (daily O_3 data is averaged at 13:00 LT and 14:00LT) exceeding 160 μg/m^3 has a large component that is due to local photochemical production, not meteorology or regional transport. We calculated for each city the monthly mean surface O_3 as function of the monthly column densities of NO_2 and HCHO for all months during May – October from 2016 to 2019. The results are shown in Figure 1c. We only consider observations of monthly HCHO columns higher than 2×10^{15} molecule/cm^2 (detection limitation), NO_2 columns more than 1.5×10^{15} molecule/cm^2 (which are defined as polluted regions) and O_3 columns above 160 μg/m^3 (minimizing the effect of background ozone). We then plot in Figure 1d the surface O_3 concentrations as function of the FNR to determine the range of FNRs, which includes the O_3 maximum for most (> 60%) cities. This range, which we define as the transition between the NO_x-limited and VOC-limited regime.

It should be noted that the actual split between NO_x-limited and VOC-limited regime includes a broad transitional region rather than a sharp dividing line (Sillman, 1999). Although we reduce the noise by gridding, there is a blurry transition between NO_x-limited and VOC-limited regimes. The lack of sharp and clear transitions between two O_3 sensitivity regimes is likely influenced by factors such as meteorology, chemical and depositional loss of O_3 and noisy satellite data. We find a relationship between FNR and the O_3 response patterns that is qualitatively similar but quantitatively distinct across cities. Taking into account the range of transitional regime, the FNR thresholds [2.3, 4.2] marking the transitional regime, are defined as the ± 30% range from the median (3.28) covering the O_3 maximum in most (60%) studied cities.

To minimize the effect of background O_3 by transport or meteorological variability, we use monthly mean O_3 concentrations above 160 μg/m^3 in summer time when the O_3 chemistry is strongest. We assume that the results are applicable for the whole of China. To check this assumption we investigate the FNR thresholds in different latitude zones (18 ℕ-28 ℕ, 28 ℕ-38 ℕ, 38 ℕ-53 ℕ) in Figure S1 in the supplement. Generally, we conclude that the derived FNR thresholds range of [2.3, 4.2] for the whole domain is a good representation for all latitude zones in China.

Figure S2(a) in the supplement shows monthly O_3 concentration in winter (Dec-Jan-Feb) which rarely exceed 160 μg/m^3, including the FNR thresholds derived using summertime data. Based on Figure S2(b) we assume that our FNR thresholds [2.3, 4.2] derived using summertime data will be valid for all seasons. Three regimes can be roughly identified from the FNR thresholds we adopted: a VOC-limited regime should occur when the FNR < 2.3 and a NO_x-limited regime should occur when the FNR > 4.2. The FNR between 2.3 and 4.2 reflects the transitions between the two regimes.

3.2 Variations of O_3 formation sensitivity in China

Figure 2a and 2b show the photochemical regime classification over China in summer of 2016 and 2019 using our FNR thresholds. Combined with the China provincial administrative division in Figure S3 in the supplement, we see the VOC-limited regimes mainly appear in the North China Plain (NCP), the Yangtze River Delta (YRD) and the Pearl River Delta (PRD), and the NO_x-limited regimes dominate the remaining areas, which are consistent with results from Wang et al. (2019a) and Jin and Holloway (2015). In the NCP, the VOC-limited regimes are found in Beijing and some big cities in Hebei province,

central regions in Shandong province and Henan province. Transitional regimes control the remaining regions of Shandong province and Henan province and most regions of Hefei province. In the YRD, the VOC-limited regimes are found in Shanghai and southern Jiangsu province. In the PRD, the VOC-limited regimes are found in Guangzhou. Outside the NCP, YRD and PRD, the VOC-limited regimes concentrate in city centers of Shenyang, Chengdu, Chongqing, Xi'an and Wuhan, that are surrounded by transitional regimes in the suburban areas. It has been acknowledged that the urban O_3 formations are generally VOC-limited due to the large amount of NO_x emissions from diverse sectors, like transportation, industry, residential sector and power plants (Shao et al., 2009; Wang et al., 2009; Sun et al., 2011). The NO_x-limited or transitional regimes dominated O_3 formation in the suburban and rural areas of eastern China (Xing et al., 2011; Jin et al., 2017).

Comparison of O_3 sensitivities between 2016 and 2019 shows noticeable changes from VOC-limited regime to transitional regime in the NCP, YRD and PRD. In the NCP, the continuous area of VOC-limited regimes that occurred in 2016 change to transitional regimes in 2019. The VOC-limited regimes remain in central Beijing, Tianjin, Shijiazhuang, Jinan and Zhengzhou. In the YRD, Shanghai and Nanjing remain in the VOC-limited regime, other cities mostly change to the transitional regime. In the PRD, the VOC-limited regime still controls Guangzhou, while the transitional regimes control its surrounding cities.

Figure 2c and 2d show mean HCHO columns over China in the summer of 2016 and 2019. The columns exceed 15×10^{15} molecule/cm^2 in megacity clusters, such as in the NCP, YRD and PRD, and the Sichuan Basin. Shen et al. (2019) found large increases of HCHO columns during May - September over 2005 - 2016 in the NCP and the YRD, consistent with the trend of anthropogenic VOC emissions. Our results show that the satellite HCHO columns increase in the NCP and the YRD and decrease in the PRD and in the Sichuan Basin during May - October of the 2016 - 2019 period. Figure 2e shows mean NO_2 columns over China in the summer of 2016. The NCP, YRD, PRD, Sichuan Basin and Urumqi have high levels (80×10^{15} molecule/cm^2) of NO_2 columns. Figure 2f shows the satellite NO_2 columns have a strong decline in the NCP, the PRD, Hunan, Hubei and Jiangxi province in summer from 2016 to 2019. However, the YRD shows increasing NO_2 columns in 2019.

We select typical cities (Beijing, Shanghai, Guangzhou, Neijiang, Lhasa and NaHa) to analyze in more detail the O_3 formation sensitivity in the summers of 2016 to 2019 in Figure 3. These cities are selected based on their different chemical regimes in 2016. The locations of the six cities are shown in Figure S4 in the supplement. Economically developed megacities or provincial capital cities such as Beijing, Shanghai and Guangzhou with high levels of tropospheric NO_2 and HCHO, remain in the VOC-limited regime over 2016-2019. The reduction of tropospheric NO_2 results in a shift in the O_3 formation sensitivity in cities such as Neijiang over 2016-2019. Lhasa as a city with low NO_2 and the background station in NaHa with even lower HCHO and NO_2 columns remain in the NO_x-limited regime over 2016-2019.

As we know, O_3 increases with increasing NO_x in the NO_x-limited regime and decreases with increasing NO_x in the VOC-limited regime. The contrast between NO_x-limited and VOC-limited regimes illustrates the difficulties involved in developing policies to reduce O_3 in NO_x polluted regions. Reductions in VOCs will only be effective in reducing O_3 if VOC-limited chemistry predominates. Reductions in NO_x will be effective only if NO_x-limited chemistry predominates and may actually increase O_3 in VOC-sensitive regions. If cities belonging to the VOC-limited regime like Beijing only focus on the reduction

of NO_x while ignore the control of VOC emissions, they will experience a process of rising O_3 concentrations, the more NO_x decrease, the greater the increase of O_3 will be.

3.3 Observed response of ground-level O_3 to chemical formation sensitivity

To validate the regimes derived from satellite observations, we also analyze the surface NO_2 observations from ground-based measurements. Figure 4a and 4b show the mean ground-based NO_2 concentrations in summer of 2016 and 2019. According to the NO_x surface emission estimates derived with DECSO from OMI observations, the NO_x emissions in eastern China (18 °N, 104 °E, 41.5 °N, 124 °E) decrease from 5.93 Tg/yr in 2016 to 4.21 Tg/yr in 2019. Such a strong decline in NO_x emissions led to decreasing ambient NO_2 concentrations at NCP (Beijing, Shijiazhuang, Zhengzhou, Jinan) and YRD (Hefei and other cities in Anhui province). In Figure 4c, the national average NO_2 concentration decrease by 14.4% in summer from 2016 to 2019.

Figure 4d and 4e show the mean ground-based O_3 concentration of about 360 cities across China in summer of 2016 and 2019. Generally, the O_3 levels in western China are lower than in eastern China. In 2016, few cities have an average O_3 concentration above 140 $\mu g/m^3$. In 2019, cities with a mean O_3 concentration exceeding 140 $\mu g/m^3$ occurred at the NCP (Tianjin, Shijiazhuang, some cities in Shandong and Henan province), the YRD (Nanjing), and the PRD (Guangzhou). In Figure 4f, we see the number of cities with average O_3 values above 140 $\mu g/m^3$ increases rapidly from 2.20% in 2016 to 31.37% in 2019. The cities with an average O_3 value below 80 $\mu g/m^3$ decrease from 11.02% in 2016 to 2.24% in 2019. In addition, the nationwide O_3 average in summer increases year by year from 2016 (104.86 $\mu g/m^3$) to 2019 (125.14 $\mu g/m^3$). Li et al. (2019a) reported the increasing O_3 trends in summer in megacity clusters of eastern China and the highest O_3 concentrations are in the NCP, which are consistent with our results.

A complex coupling of primary emissions, chemical transformation, and dynamic transport at different scales determine the O_3 pollution (Jacob, 1999). NO_x and VOCs play important roles in O_3 formation. Emissions of NO_x and VOCs to the environment are the starting point of O_3 pollution problems. During the past decade in China, ambitious steps have been taken to control NO_x emissions. In 2013, the Chinese State Council issued the APPAP. Stringent control measures were carried out since then, including phasing out high-emitting industries, closing outdated factories, tightening industrial emission standard, improving fuel quality (Wang et al., 2019a). However, to the other important O_3 precursors, VOCs, less attention has been given in emission control strategy. Li et al. (2019b) concluded that anthropogenic NMVOC emissions in China during 1990-2017 have been increasing continuously due to the dramatic growth in activity rates and absence of effective control measures. Following China's past control strategy on VOCs, we can regard VOC emissions as rising or in steady state.

The reduction of the NO_x emissions for cities in the VOC-limited regime is one of the main reason for the increasing of O_3. Figure 5a shows the difference of total NO_x emissions derived from OMI observations in summer in east China between 2019 and 2016. A decline in NO_x emissions centers at the NCP, YRD and PRD, where most areas belong to the VOC-limited regime. In order to provide further insight into the impact of NO_x emission variations on O_3 concentrations, five selected typical cities (Beijing, Shanghai, Guangzhou, Neijiang and NaHa) are shown in more detail (see Figure 5b and 5c). For cities

under the control of VOC-limited chemistry (Beijing, Shanghai and Guangzhou), accompanied with decreasing NO_x emissions, O_3 concentrations generally show an opposite behavior to NO_x emissions. The O_3 formation sensitivity in Neijiang shows a shift from the transitional to the NO_x-limited regime over 2016-2019. The reduction of NO_x emissions in the transitional regime is accompanied by decreasing O_3 in Neijiang. Although the O_3 data in NaHa for 2016-2018 are unavailable, we see that O_3 concentrations in NaHa are low in 2019 and NO_x emissions are stable during 2016-2019. Note that we find a qualitative relationship between NO_x emission and the O_3 response patterns conform the nonlinear O_3-NO_2-VOC chemistry, not in quantitative sense. For example, the changes of NO_x emissions in Beijing (-2.17 Gg N/cell), Shanghai (-1.18 Gg N/cell), Guangzhou (-0.28 Gg N/cell) and Neijiang (-0.15 Gg N/cell) during 2016-2019 lead to different levels of O_3 changes in Beijing (10.43 $\mu g/m^3$), Shanghai (7.81 $\mu g/m^3$), Guangzhou (25.54 $\mu g/m^3$) and Neijiang (-22.66 $\mu g/m^3$). Because of the VOC-limited chemistry condition, O_3 increases with decreasing NO_x emissions in Beijing, Shanghai and Guangzhou. The NO_x-limited condition leads to decreasing O_3 with decreasing NO_x emissions in Neijiang. Compared with Beijing, NO_x emissions in Guangzhou remained basically constant in 2016 and 2019. But O_3 concentrations in Guangzhou increased more than in Beijing. The local O_3 formation sensitivity is helpful to present the way of O_3 response to NO_x emission, but VOC emission are needed when discussing their relationship in a quantitative way.

3.4 Enhanced O_3 levels during COVID-19 lockdown in China

The measures in response to the outbreak of the COVID-19 lead to sudden changes of NO_x emissions and anthropogenic HCHO emissions in China in the beginning of 2020 (Wang et al., 2020; Hui et al., 2020). We analyze the change of O_3 concentrations during the lockdown period to validate our method. To look into COVID-19 lockdown impacts on short-term O_3 level, we choose two time periods covering 357 cities across China: period I (3 - 23 January, 2020) and period II (9 - 29 February, 2020), to avoid the coincidence of Chinese New Year holidays (24 January to 8 February, 2020).

Figure 6a shows enhanced O_3 levels in most cities of eastern China during the COVID-19 lockdown, except for some cities in PRD and Fujian province. The cities with O_3 concentration increases of more than 40 $\mu g/m^3$ are located in the NCP and the YRD, the populous regions of China, indicating a potential negative health effect from O_3 exposure in these regions. Figure 6b shows strong reductions in NO_x emissions in eastern China, especially in Henan, Hubei and Jiangsu province, where as a consequence of the lockdown, transportation, construction, and light industry activities have been dramatically decreased.

Assuming that our observation-based FNR thresholds derived using summertime data also apply during winter, we see that most regions of eastern China belong to the VOC-limited regime during period I and II in Figure 6c and 6d. Previous studies also reported that the O_3 chemistry in the urban areas in China in wintertime is in a VOC-limited regime due to the relative lack of HO_x radicals (Seinfeld and Pandis, 2016). During winter (VOC-limited conditions), when the concentration of NO_x is high, and the level of UV radiation is low, the O_3 production varies inversely with the NO_x concentration (Sillman et al., 1990). During the lockdown period, both the anthropogenic emissions of NO_x and VOCs were reduced. The NO_x reduction during the lockdown is higher than the VOC reduction according to Sicard et al. (2020). The reductions of VOC emissions are generally effective in reducing O_3 concentrations. However, such air quality improvements are largely offset by reductions in

NO_x emissions leading to increases in O_3 concentrations due to the strongly VOC-limited conditions in the NCP in winter (Xing et al., 2020). The NO_x reduction during the lockdown is higher than the VOC reduction (Sicard et al., 2020). Thus, a reduction in NO_x leads to an increase of the O_3 concentrations in most regions of eastern China during period II. Besides, reduction of freshly emitted NO in particular from road traffic alleviates O_3 titration locally (Seinfeld and Pandis, 2016; Levy et al., 2014). The O_3 titration occurs particularly in winter (less photolysis reactions of NO_2) under high NO_x levels (Sillman, 1999). However, the lockdown measures result primarily in a lower titration of O_3 by NO due to the reduction in local NO_x emissions by road transport, which also enhances O_3 levels in urban areas. On the other hand, some cities, mainly located in southeastern China, showed decreasing O_3 levels. Zhao et al. (2020) concluded that the cause of O_3 decline in these cities is the emission changes of NO_x and VOC. In Figure 6c we see that some cities in Fujian and Guangdong provinces belong to the transitional regime. Theoretically, the transitional regime should correspond to the conditions at which O_3 formation is most efficient, indicating that reductions or increases in NO_x and VOCs will reduce the O_3 concentration.

4 Conclusion

Satellite-based $HCHO/NO_2$ ratios and ground-based O_3 measurements were directly connected to capture the non-linearity of surface O_3 chemistry over major Chinese cities in this study. Evaluating the FNR thresholds marking the O_3 transitional regime in which O_3 formation is less sensitive to the precursors, we found a broad transitional region, which reflects differences of factors among 360 cities, such as emissions, meteorology, and regional transport. The national FNR thresholds are defined as follows: a VOC-limited regime should occur for FNR < 2.3 and a NO_x-limited regime should occur for FNR > 4.2. The FNR between 2.3 and 4.2 reflects the transition between the two regimes. Our FNR thresholds derived from satellite and ground-based observations are higher than previous reported model-based values. The nonlinear chemistry of O_3 depends on its precursors NO_2 and VOCs with contributions from both local and regional sources (Xue et al., 2014). Modeling studies are good at simulating the response of surface O_3 to an overall reduction in NO_x or VOC emissions. The FNR thresholds derived with *in situ* O_3 observations will be more indicative of the local O_3 chemistry than the model, including the effect of NO_x titration over urban areas (Jin et al., 2020).

We analyzed the spatial and temporal variability of O_3 formation sensitivity using our FNR thresholds over China from 2016 to 2019. Our results showed that O_3 formation sensitivity tends to be VOC-limited over urban areas and NO_x-limited over rural and remote areas in China. In 2016, the VOC-limited regimes mainly appear in the NCP, the YRD and the PRD. In 2019, there was a shift in most NCP regions from the VOC-limited to the transitional regime. The area with a VOC-limited regime in the YRD and PRD also shrank. We found that O_3 formation sensitivity changes in these regions were associated with a strong decline in tropospheric NO_2 columns in the NCP and the PRD. For megacities such as Beijing and Guangzhou, although they remained in VOC-limited regime over 2016-2019, there was still a decrease in NO_2 columns. Consistent with decreasing tropospheric NO_2 columns, the national average surface NO_2 concentration decreased by 14.4% in summer from 2016 to 2019 and the NO_x emissions in eastern China decreased from 5.93 Tg/yr in 2016 to 4.21 Tg/yr in 2019. This detected

spatial expansion of the transitional regime and NO_x emission reduction in VOC-limited regime has contributed to rising surface O_3 concentrations. The nationwide averaged O_3 concentration in summer increased year by year from 2016 (104.86 $\mu g/m^3$) to 2019 (125.14 $\mu g/m^3$). The cities with average O_3 values above 140 $\mu g/m^3$ increased rapidly from 2.20% in 2016 to 31.37% in 2019.

Satellite instruments measure the vertically integrated column density, which we use as a proxy of the actual surface concentrations. To reduce the effect of short-term variability in vertical distributions caused by meteorological changes we use monthly mean averages. Therefore, our satellite-based $HCHO/NO_2$ method is limited to identification of long-term evolution in O_3 sensitivity, focusing on understanding the average air quality.

We presented the level of O_3 formed from photo-oxidation of total measured HCHO only, not differentiating the contributions from different sources (directly emitted or photochemical formed). Due to the higher temperature and stronger solar radiation in summer, the higher concentration level of HCHO mainly results from the intense photo-oxidation of VOCs. Emission sources of HCHO, as a tracer of VOCs, can be anthropogenic and biogenic. Shen et al. (2019) found that the OMI HCHO distribution follows their anthropogenic inventory in megacity clusters over China, while it does not follow the biogenic emissions inventory. Despite the fact that local sources of anthropogenic VOCs are difficult to identify, our FNR thresholds derived from satellite-based information have the potential to provide important information to air quality planners. Compared with stringent control measures for NO_x emissions, VOC emissions got less attention as the other O_3 precursor in China. The case study of O_3 level changes during the COVID-19 lockdown in China demonstrated that the strong reductions in anthropogenic NO_x emissions resulted in significant O_3 enhancement due to the VOC-limited regime in winter. It indicates that a protocol with strict measures to control NO_x emissions, without simultaneous VOC emissions controls for power plants and heavy industry, such as petrochemical facilities, achieves only limited effects on O_3 pollution.

Data availability

Satellite data used in this research can be obtained from public sources. The OMI tropospheric NO_2 product from the QA4ECV project can be obtained from http://www.qa4ecv.eu/ecv/no2-pre/data and the HCHO product from http://www.qa4ecv.eu/ecv/hcho-p/data.

The monthly mean NO_x emission products derived from OMI observations by DECSO v5.1qa can be obtained from https://www.temis.nl/emissions/region_asia/datapage.php.

The hourly O_3 and NO_2 observations of Chinese ground stations can be accessed from third parties (http://www.pm25.in, http://www.aqicn.org).

The hourly O_3 and NO_2 observations of Naha station are provided by the Japanese Atmospheric Environmental Regional Observation System (AEROS, http://soramame.taiki.go.jp/Index.php).

Author contributions

WW and RA provided satellite data, tools, and analysis. RA, JD, MW and TC undertook the conceptualization and investigation. WW prepared original draft. RA and JD carried out review and editing. All authors discussed the results and commented on the paper.

Competing interests

The authors declare that they have no conflict of interest.

Acknowledgements

The support provided by China Scholarship Council (CSC) during a visit of Wannan Wang to Royal Netherlands Meteorological Institute (KNMI) is acknowledged.

References

Barbaro, E., de Arellano, J. V.-G., Ouwersloot, H. G., Schröter, J. S., Donovan, D. P., and Krol, M. C.: Aerosols in the convective boundary layer: Shortwave radiation effects on the coupled land-atmosphere system, 119, 5845-5863, 10.1002/2013jd021237, 2014.

Bauwens, M., Compernolle, S., Stavrakou, T., Müller, J. F., van Gent, J., Eskes, H., Levelt, P. F., van der A, R., Veefkind, J. P., Vlietinck, J., Yu, H., and Zehner, C.: Impact of Coronavirus Outbreak on NO2 Pollution Assessed Using TROPOMI and OMI Observations, Geophysical Research Letters, 47, e2020GL087978, 10.1029/2020GL087978, 2020.

Boersma, K. F., Eskes, H. J., Richter, A., De Smedt, I., Lorente, A., Beirle, S., van Geffen, J. H. G. M., Zara, M., Peters, E., Van Roozendael, M., Wagner, T., Maasakkers, J. D., van der A, R. J., Nightingale, J., De Rudder, A., Irie, H., Pinardi, G., Lambert, J. C., and Compernolle, S. C.: Improving algorithms and uncertainty estimates for satellite NO2 retrievals: results from the quality assurance for the essential climate variables (QA4ECV) project, Atmos. Meas. Tech., 11, 6651-6678, 10.5194/amt-11-6651-2018, 2018.

Boersma, K. F., Braak. K., and van der A, R. J.: Dutch OMI NO2 (DOMINO) data product v2.0 HE5 data file user manual, available at: https://d37onar3vnbj2y.cloudfront.net/static/docs/OMI_NO2_HE5_2.0_2011.pdf, 2011,

Brown-Steiner, B., Hess, P. G., and Lin, M. Y.: On the capabilities and limitations of GCCM simulations of summertime regional air quality: A diagnostic analysis of ozone and temperature simulations in the US using CESM CAM-Chem, Atmospheric Environment, 101, 134-148, https://doi.org/10.1016/j.atmosenv.2014.11.001, 2015.

Cai, S., Wang, Y., Zhao, B., Wang, S., Chang, X., and Hao, J.: The impact of the "Air Pollution Prevention and Control Action Plan" on PM2.5 concentrations in Jing-Jin-Ji region during 2012–2020, Science of The Total Environment, 580, 197-209, https://doi.org/10.1016/j.scitotenv.2016.11.188, 2017.

Cheng, L., Wang, S., Gong, Z., Li, H., Yang, Q., and Wang, Y.: Regionalization based on spatial and seasonal variation in ground-level ozone concentrations across China, Journal of Environmental Sciences, 67, 179-190, https://doi.org/10.1016/j.jes.2017.08.011, 2018.

Chinese Ministry of Ecology and Environment (CMEE)., Technical Specifications for Installation and Acceptance of Ambient air Quality Continuous Automated Monitoring System for SO2, NO2, O3 and CO. Available at http://www.mee.gov.cn/ywgz/fgbz/bz/bzwb/jcffbz/201308/W020130802493970989627.pdf. Accessed: 3th February 2021.

Choi, Y., Kim, H., Tong, D., and Lee, P.: Summertime weekly cycles of observed and modeled NO_x and O_3 concentrations as a function of satellite-derived ozone production sensitivity and land use types over the Continental United States, Atmos. Chem. Phys., 12, 6291-6307, 10.5194/acp-12-6291-2012, 2012.

Choi, Y., and Souri, A. H.: Chemical condition and surface ozone in large cities of Texas during the last decade: Observational evidence from OMI, CAMS, and model analysis, Remote Sensing of Environment, 168, 90-101, https://doi.org/10.1016/j.rse.2015.06.026, 2015.

Chou, C. C. K., Tsai, C. Y., Chang, C. C., Lin, P. H., Liu, S. C., and Zhu, T.: Photochemical production of ozone in Beijing during the 2008 Olympic Games, Atmos. Chem. Phys., 11, 9825-9837, 10.5194/acp-11-9825-2011, 2011.

Announcement on Issuing the Amendment of 'Ambient Air Quality Standard' (GB 3095-2012): http://www.mee.gov.cn/gkml/sthjbgw/sthjbgg/201808/t20180815_451398.htm, access: 24 June, 2018.

Crutzen, P. J.: Photochemical reactions initiated by and influencing ozone in unpolluted tropospheric air, Tellus, 26, 47-57, 10.3402/tellusa.v26i1-2.9736, 1974.

Ding, A. J., Fu, C. B., Yang, X. Q., Sun, J. N., Petäjä, T., Kerminen, V. M., Wang, T., Xie, Y., Herrmann, E., Zheng, L. F., Nie, W., Liu, Q., Wei, X. L., and Kulmala, M.: Intense atmospheric pollution modifies weather: a case of mixed biomass burning with fossil fuel combustion pollution in eastern China, Atmos. Chem. Phys., 13, 10545-10554, 10.5194/acp-13-10545-2013, 2013.

Ding, J., van der A, R. J., Mijling, B., Levelt, P. F., and Hao, N.: NO_x emission estimates during the 2014 Youth Olympic Games in Nanjing, Atmos. Chem. Phys., 15, 9399-9412, 10.5194/acp-15-9399-2015, 2015.

Ding, J., van der A, R. J., Mijling, B., and Levelt, P. F.: Space-based NO_x emission estimates over remote regions improved in DECSO, Atmos. Meas. Tech., 10, 925-938, 10.5194/amt-10-925-2017, 2017.

Ding, J., van der A, R. J., Mijling, B., Jalkanen, J. P., Johansson, L., and Levelt, P. F.: Maritime NO_x Emissions Over Chinese Seas Derived From Satellite Observations, Geophysical Research Letters, 45, 2031-2037, 10.1002/2017GL076788, 2018.

Ding, J., van der A, R. J., Eskes, H., Mijling, B., Stavrakou, T., Geffen, J., and Veefkind, P.: NO_x emissions reduction and rebound in China due to the COVID-19 crisis, Geophysical Research Letters., https://doi.org/10.1002/essoar.10503971.1, 2020.

Duncan, B. N., Yoshida, Y., Olson, J. R., Sillman, S., Martin, R. V., Lamsal, L., Hu, Y., Pickering, K. E., Retscher, C., and Allen, D. J. J. A. E.: Application of OMI observations to a space-based indicator of NO_x and VOC controls on surface ozone formation, 44, 2213-2223, 2010.

Feng, L., and Liao, W.: Legislation, plans, and policies for prevention and control of air pollution in China: achievements, challenges, and improvements, Journal of Cleaner Production, 112, 1549-1558, https://doi.org/10.1016/j.jclepro.2015.08.013, 2016.

Fishman, J., Ramanathan, V., Crutzen, P. J., and Liu, S. C.: Tropospheric ozone and climate, Nature, 282, 818-820, 10.1038/282818a0, 1979.

Fu, T.-M., Jacob, D. J., Palmer, P. I., Chance, K., Wang, Y. X., Barletta, B., Blake, D. R., Stanton, J. C., and Pilling, M. J.: Space-based formaldehyde measurements as constraints on volatile organic compound emissions in east and south Asia and implications for ozone, 112, 10.1029/2006jd007853, 2007.

Hammer, M.-U., Vogel, B., and Vogel, H.: Findings on H_2O_2/HNO_3 as an indicator of ozone sensitivity in Baden-Württemberg, Berlin-Brandenburg, and the Po valley based on numerical simulations, 107, LOP 3-1-LOP 3-18, 10.1029/2000jd000211, 2002.

Huang, J., Li, G., Xu, G., Qian, X., Zhao, Y., Pan, X., Huang, J., Cen, Z., Liu, Q., He, T., and Guo, X.: The burden of ozone pollution on years of life lost from chronic obstructive pulmonary disease in a city of Yangtze River Delta, China, Environmental Pollution, 242, 1266-1273, https://doi.org/10.1016/j.envpol.2018.08.021, 2018.

Huang, X., Ding, A., Gao, J., Zheng, B., Zhou, D., Qi, X., Tang, R., Wang, J., Ren, C., Nie, W., Chi, X., Xu, Z., Chen, L., Li, Y., Che, F., Pang, N., Wang, H., Tong, D., Qin, W., Cheng, W., Liu, W., Fu, Q., Liu, B., Chai, F., Davis, S. J., Zhang, Q., and He, K.: Enhanced secondary pollution offset reduction of primary emissions during COVID-19 lockdown in China, National Science Review, 10.1093/nsr/nwaa137, 2020.

Hui, D. S., I Azhar, E., Madani, T. A., Ntoumi, F., Kock, R., Dar, O., Ippolito, G., McHugh, T. D., Memish, Z. A., Drosten, C., Zumla, A., and Petersen, E.: The continuing 2019-nCoV epidemic threat of novel coronaviruses to global health — The latest 2019 novel coronavirus outbreak in Wuhan, China, International Journal of Infectious Diseases, 91, 264-266, https://doi.org/10.1016/j.ijid.2020.01.009, 2020.

IPCC: Climate Change 2013 – The Physical Science Basis: Working Group I Contribution to the Fifth Assessment Report of the Intergovernmental Panel on Climate Change, Cambridge University Press, Cambridge, 2014.

Jacob, D. J.: Introduction to Atmospheric Chemistry, Princeton University Press, 1999.

Jacob, D. J.: Heterogeneous chemistry and tropospheric ozone, Atmospheric Environment, 34, 2131-2159, https://doi.org/10.1016/S1352-2310(99)00462-8, 2000.

Janssen, R. H. H., Vil à-Guerau de Arellano, J., Ganzeveld, L. N., Kabat, P., Jimenez, J. L., Farmer, D. K., van Heerwaarden, C. C., and Mammarella, I.: Combined effects of surface conditions, boundary layer dynamics and chemistry on diurnal SOA evolution, Atmos. Chem. Phys., 12, 6827-6843, 10.5194/acp-12-6827-2012, 2012.

Jeon, W., Choi, Y., Souri, A. H., Roy, A., Diao, L., Pan, S., Lee, H. W., and Lee, S.-H.: Identification of chemical fingerprints in long-range transport of burning induced upper tropospheric ozone from Colorado to the North Atlantic Ocean, Science of The Total Environment, 613-614, 820-828, https://doi.org/10.1016/j.scitotenv.2017.09.177, 2018.

Jerrett, M., Burnett, R. T., Pope, C. A., Ito, K., Thurston, G., Krewski, D., Shi, Y., Calle, E., and Thun, M.: Long-Term Ozone Exposure and Mortality, 360, 1085-1095, 10.1056/NEJMoa0803894, 2009.

Jin, X., and Holloway, T.: Spatial and temporal variability of ozone sensitivity over China observed from the Ozone Monitoring Instrument, 120, 7229-7246, 10.1002/2015jd023250, 2015.

Jin, X., Fiore, A. M., Murray, L. T., Valin, L. C., Lamsal, L. N., Duncan, B., Folkert Boersma, K., De Smedt, I., Abad, G. G., Chance, K., and Tonnesen, G. S.: Evaluating a Space-Based Indicator of Surface Ozone-NOx-VOC Sensitivity Over Midlatitude Source Regions and Application to Decadal Trends, Journal of Geophysical Research: Atmospheres, 122, 10,439-410,461, 10.1002/2017JD026720, 2017.

Jin, X., Fiore, A., Boersma, K. F., Smedt, I. D., and Valin, L.: Inferring Changes in Summertime Surface Ozone–NOx–VOC Chemistry over U.S. Urban Areas from Two Decades of Satellite and Ground-Based Observations, Environmental Science & Technology, 54, 6518-6529, 10.1021/acs.est.9b07785, 2020.

Khaniabadi, Y. O., Hopke, P. K., Goudarzi, G., Daryanoosh, S. M., Jourvand, M., and Basiri, H.: Cardiopulmonary mortality and COPD attributed to ambient ozone, Environmental Research, 152, 336-341, https://doi.org/10.1016/j.envres.2016.10.008, 2017.

Kleinman, L.: Low and high NOx tropospheric photochemistry, Journal of Geophysical Research: Atmospheres, 99, 16831-16838, 1994.

Kurokawa, J., Ohara, T., Morikawa, T., Hanayama, S., Janssens-Maenhout, G., Fukui, T., Kawashima, K., and Akimoto, H.: Emissions of air pollutants and greenhouse gases over Asian regions during 2000–2008: Regional Emission inventory in ASia (REAS) version 2, Atmos. Chem. Phys., 13, 11019-11058, 10.5194/acp-13-11019-2013, 2013.

Lamsal, L. N., Krotkov, N. A., Celarier, E. A., Swartz, W. H., Pickering, K. E., Bucsela, E. J., Gleason, J. F., Martin, R. V., Philip, S., Irie, H., Cede, A., Herman, J., Weinheimer, A., Szykman, J. J., and Knepp, T. N.: Evaluation of OMI operational

standard NO_2 column retrievals using in situ and surface-based NO_2 observations, Atmos. Chem. Phys., 14, 11587-11609, 10.5194/acp-14-11587-2014, 2014.

Levelt, P. F., Oord, G. H. J. v. d., Dobber, M. R., Malkki, A., Huib, V., Johan de, V., Stammes, P., Lundell, J. O. V., and Saari, H.: The ozone monitoring instrument, IEEE Transactions on Geoscience and Remote Sensing, 44, 1093-1101, 2006.

Levy, M., Zhang, R., Zheng, J., Zhang, A. L., Xu, W., Gomez-Hernandez, M., Wang, Y., and Olaguer, E.: Measurements of nitrous acid (HONO) using ion drift-chemical ionization mass spectrometry during the 2009 SHARP field campaign, Atmospheric Environment, 94, 231-240, https://doi.org/10.1016/j.atmosenv.2014.05.024, 2014.

Li, K., Jacob, D. J., Liao, H., Shen, L., Zhang, Q., and Bates, K. H.: Anthropogenic drivers of 2013–2017 trends in summer surface ozone in China, Proceedings of the National Academy of Sciences, 116, 422, 10.1073/pnas.1812168116, 2019a.

Li, M., Zhang, Q., Kurokawa, J. I., Woo, J. H., He, K., Lu, Z., Ohara, T., Song, Y., Streets, D. G., Carmichael, G. R., Cheng, Y., Hong, C., Huo, H., Jiang, X., Kang, S., Liu, F., Su, H., and Zheng, B.: MIX: a mosaic Asian anthropogenic emission inventory under the international collaboration framework of the MICS-Asia and HTAP, Atmos. Chem. Phys., 17, 935-963, 10.5194/acp-17-935-2017, 2017.

Li, M., Zhang, Q., Zheng, B., Tong, D., Lei, Y., Liu, F., Hong, C., Kang, S., Yan, L., Zhang, Y., Bo, Y., Su, H., Cheng, Y., and He, K.: Persistent growth of anthropogenic non-methane volatile organic compound (NMVOC) emissions in China during 1990–2017: drivers, speciation and ozone formation potential, Atmos. Chem. Phys., 19, 8897-8913, 10.5194/acp-19-8897-2019, 2019b.

Li, P., De Marco, A., Feng, Z., Anav, A., Zhou, D., and Paoletti, E.: Nationwide ground-level ozone measurements in China suggest serious risks to forests, Environmental Pollution, 237, 803-813, https://doi.org/10.1016/j.envpol.2017.11.002, 2018.

Li, X., Zhang, C., Zhang, B., and Liu, K.: A comparative time series analysis and modeling of aerosols in the contiguous United States and China, Science of The Total Environment, 690, 799-811, https://doi.org/10.1016/j.scitotenv.2019.07.072, 2019c.

Liu, Z., Wang, Y., Gu, D., Zhao, C., Huey, L. G., Stickel, R., Liao, J., Shao, M., Zhu, T., Zeng, L., Amoroso, A., Costabile, F., Chang, C. C., and Liu, S. C.: Summertime photochemistry during CAREBeijing-2007: RO_x budgets and O_3 formation, Atmos. Chem. Phys., 12, 7737-7752, 10.5194/acp-12-7737-2012, 2012.

Martin, R. V., Fiore, A. M., and Van Donkelaar, A.: Space-based diagnosis of surface ozone sensitivity to anthropogenic emissions, 31, 10.1029/2004gl019416, 2004.

Mijling, B., and van der A, R. J.: Using daily satellite observations to estimate emissions of short-lived air pollutants on a mesoscopic scale, Journal of Geophysical Research: Atmospheres, 117, 10.1029/2012JD017817, 2012.

Milford, J. B., Russell, A. G., and McRae, G. J.: A new approach to photochemical pollution control: Implications of spatial patterns in pollutant responses to reductions in nitrogen oxides and reactive organic gas emissions, Environmental Science Technology, 23, 1290-1301, 1989.

Millet, D. B., Jacob, D. J., Boersma, K. F., Fu, T.-M., Kurosu, T. P., Chance, K., Heald, C. L., and Guenther, A.: Spatial distribution of isoprene emissions from North America derived from formaldehyde column measurements by the OMI satellite sensor, 113, 10.1029/2007jd008950, 2008.

Palmer, P. I., Jacob, D. J., Fiore, A. M., Martin, R. V., Chance, K., and Kurosu, T. P.: Mapping isoprene emissions over North America using formaldehyde column observations from space, 108, 10.1029/2002jd002153, 2003.

Schroeder, J. R., Crawford, J. H., Fried, A., Walega, J., Weinheimer, A., Wisthaler, A., Müller, M., Mikoviny, T., Chen, G., Shook, M., Blake, D. R., and Tonnesen, G. S.: New insights into the column CH_2O/NO_2 ratio as an indicator of near-surface ozone sensitivity, Journal of Geophysical Research: Atmospheres, 122, 8885-8907, 10.1002/2017JD026781, 2017.

Seinfeld, J. H., and Pandis, S. N.: Atmospheric Chemistry and Physics: From Air Pollution to Climate Change, Wiley, 2016.

Shah, V., Jacob, D. J., Li, K., Silvern, R. F., Zhai, S., Liu, M., Lin, J., and Zhang, Q.: Effect of changing NO_x lifetime on the seasonality and long-term trends of satellite-observed tropospheric NO_2 columns over China, Atmos. Chem. Phys., 20, 1483-1495, 10.5194/acp-20-1483-2020, 2020.

Shao, M., Zhang, Y., Zeng, L., Tang, X., Zhang, J., Zhong, L., and Wang, B.: Ground-level ozone in the Pearl River Delta and the roles of VOC and NO_x in its production, Journal of Environmental Management, 90, 512-518, https://doi.org/10.1016/j.jenvman.2007.12.008, 2009.

Shen, L., Jacob, D. J., Zhu, L., Zhang, Q., Zheng, B., Sulprizio, M. P., Li, K., De Smedt, I., González Abad, G., Cao, H., Fu, T.-M., and Liao, H.: The 2005–2016 Trends of Formaldehyde Columns Over China Observed by Satellites: Increasing Anthropogenic Emissions of Volatile Organic Compounds and Decreasing Agricultural Fire Emissions, Geophysical Research Letters, 46, 4468-4475, 10.1029/2019GL082172, 2019.

Sicard, P., De Marco, A., Agathokleous, E., Feng, Z., Xu, X., Paoletti, E., Rodriguez, J. J. D., and Calatayud, V.: Amplified ozone pollution in cities during the COVID-19 lockdown, Science of The Total Environment, 735, 139542, https://doi.org/10.1016/j.scitotenv.2020.139542, 2020.

Siciliano, B., Dantas, G., da Silva, C. M., and Arbilla, G.: Increased ozone levels during the COVID-19 lockdown: Analysis for the city of Rio de Janeiro, Brazil, Science of The Total Environment, 737, 139765, https://doi.org/10.1016/j.scitotenv.2020.139765, 2020.

Sillman, S., Logan, J. A., and Wofsy, S. C.: The sensitivity of ozone to nitrogen oxides and hydrocarbons in regional ozone episodes, Journal of Geophysical Research: Atmospheres, 95, 1837-1851, 10.1029/JD095iD02p01837, 1990.

Sillman, S.: The use of NO_y, H_2O_2, and HNO_3 as indicators for ozone-NO_x-hydrocarbon sensitivity in urban locations, J. Geophys. Res., 100(D7), 14175– 14188, doi:10.1029/94JD02953, 1995.Sillman, S.: The relation between ozone, NO_x and hydrocarbons in urban and polluted rural environments, Atmospheric Environment, 33, 1821-1845, https://doi.org/10.1016/S1352-2310(98)00345-8, 1999.

Sillman, S.: Tropospheric Ozone and Photochemical Smog, in: Treatise on Geochemistry, edited by: Holland, H. D., and Turekian, K. K., Pergamon, Oxford, 407-431, 2003.

Smedt, I. D., Geffen, J., Richter, A., Beirle, S., Yu, H., Vlietinck, J., Roozendael, M., Lorente, A., Scanlon, T., Compernolle, S., Wagner, T., Eskes, H., and Boersma, F.: Product User Guide for HCHO, 2017.

Souri, A. H., Choi, Y., Jeon, W., Woo, J. H., Zhang, Q., and Kurokawa, J.: Remote sensing evidence of decadal changes in major tropospheric ozone precursors over East Asia, Journal of Geophysical Research: Atmospheres, 122, 2474-2492, 10.1002/2016JD025663, 2017.

Sun, Y., Wang, L., Wang, Y., Quan, L., and Zirui, L.: In situ measurements of SO_2, NO_x, NO_y, and O_3 in Beijing, China during August 2008, Science of The Total Environment, 409, 933-940, https://doi.org/10.1016/j.scitotenv.2010.11.007, 2011.

Tang, G., Wang, Y., Li, X., Ji, D., Hsu, S., and Gao, X.: Spatial-temporal variations in surface ozone in Northern China as observed during 2009–2010 and possible implications for future air quality control strategies, Atmos. Chem. Phys., 12, 2757-2776, 10.5194/acp-12-2757-2012, 2012.

Tian, H., Liu, Y., Li, Y., Wu, C.-H., Chen, B., Kraemer, M. U. G., Li, B., Cai, J., Xu, B., Yang, Q., Wang, B., Yang, P., Cui, Y., Song, Y., Zheng, P., Wang, Q., Bjornstad, O. N., Yang, R., Grenfell, B. T., Pybus, O. G., and Dye, C.: An investigation of transmission control measures during the first 50 days of the COVID-19 epidemic in China, Science, 368, 638, 10.1126/science.abb6105, 2020a.

Tian, Y., Wu, Y., Liu, H., Si, Y., Wu, Y., Wang, X., Wang, M., Wu, J., Chen, L., Wei, C., Wu, T., Gao, P., and Hu, Y.: The impact of ambient ozone pollution on pneumonia: A nationwide time-series analysis, Environment International, 136, 105498, https://doi.org/10.1016/j.envint.2020.105498, 2020b.

Tobías, A., Carnerero, C., Reche, C., Massagué, J., Via, M., Minguillón, M. C., Alastuey, A., and Querol, X.: Changes in air quality during the lockdown in Barcelona (Spain) one month into the SARS-CoV-2 epidemic, Science of The Total Environment, 726, 138540, https://doi.org/10.1016/j.scitotenv.2020.138540, 2020.

van Donkelaar, A., Martin Randall, V., Brauer, M., Kahn, R., Levy, R., Verduzco, C., and Villeneuve Paul, J.: Global Estimates of Ambient Fine Particulate Matter Concentrations from Satellite-Based Aerosol Optical Depth: Development and Application, Environmental Health Perspectives, 118, 847-855, 10.1289/ehp.0901623, 2010.

van Heerwaarden, C. C., Vilà-Guerau de Arellano, J., Gounou, A., Guichard, F., and Couvreux, F.: Understanding the Daily Cycle of Evapotranspiration: A Method to Quantify the Influence of Forcings and Feedbacks, Journal of Hydrometeorology, 11, 1405-1422, 10.1175/2010JHM1272.1, 2010.

van Stratum, B. J. H., Vilà-Guerau de Arellano, J., Ouwersloot, H. G., van den Dries, K., van Laar, T. W., Martinez, M., Lelieveld, J., Diesch, J. M., Drewnick, F., Fischer, H., Hosaynali Beygi, Z., Harder, H., Regelin, E., Sinha, V., Adame, J. A., Sörgel, M., Sander, R., Bozem, H., Song, W., Williams, J., and Yassaa, N.: Case study of the diurnal variability of chemically active species with respect to boundary layer dynamics during DOMINO, Atmos. Chem. Phys., 12, 5329-5341, 10.5194/acp-12-5329-2012, 2012.

Vilà-Guerau de Arellano, J., Patton, E. G., Karl, T., van den Dries, K., Barth, M. C., and Orlando, J. J.: The role of boundary layer dynamics on the diurnal evolution of isoprene and the hydroxyl radical over tropical forests, J. Geophys. Res., 116, D07304, 10.1029/2010JD014857, 2011.

Vilà-Guerau de Arellano, J., van Heerwaarden, C.C., van Stratum, B. J. H., and van den Dries, K.: Atmospheric Boundary Layer, Integrating Air Chemistry and Land Interactions, Cambridge University Press, New York, NY, USA. Hardcover, 265 pp, 2015.

Wang, C., Huang, X.-F., Han, Y., Zhu, B., He, L.-Y.: Sources and potential photochemical roles of formaldehyde in an urban atmosphere in South China. J. Geophys. Res., 122, 11,934–11,947. https://doi.org/10.1002/2017JD027266, 2017.

Wang, C., Horby, P. W., Hayden, F. G., and Gao, G. F.: A novel coronavirus outbreak of global health concern, The Lancet, 395, 470-473, https://doi.org/10.1016/S0140-6736(20)30185-9, 2020.

Wang, N., Lyu, X., Deng, X., Huang, X., Jiang, F., and Ding, A.: Aggravating O_3 pollution due to NO_x emission control in eastern China, Science of The Total Environment, 677, 732-744, 2019a.

Wang, Q., and Su, M.: A preliminary assessment of the impact of COVID-19 on environment – A case study of China, Science of The Total Environment, 728, 138915, https://doi.org/10.1016/j.scitotenv.2020.138915, 2020.

Wang, T., Wei, X. L., Ding, A. J., Poon, C. N., Lam, K. S., Li, Y. S., Chan, L. Y., and Anson, M.: Increasing surface ozone concentrations in the background atmosphere of Southern China, 1994–2007, Atmos. Chem. Phys., 9, 6217-6227, 10.5194/acp-9-6217-2009, 2009.

Wang, T., Xue, L., Brimblecombe, P., Lam, Y. F., Li, L., and Zhang, L.: Ozone pollution in China: A review of concentrations, meteorological influences, chemical precursors, and effects, Science of The Total Environment, 575, 1582-1596, https://doi.org/10.1016/j.scitotenv.2016.10.081, 2017a.

Wang, W. N., Cheng, T. H., Gu, X. F., Chen, H., Guo, H., Wang, Y., Bao, F. W., Shi, S. Y., Xu, B. R., Zuo, X., Meng, C., and Zhang, X. C.: Assessing Spatial and Temporal Patterns of Observed Ground-level Ozone in China, Scientific Reports, 7, 3651, 10.1038/s41598-017-03929-w, 2017b.

Wang, Z., Lv, J., Tan, Y., Guo, M., Gu, Y., Xu, S., and Zhou, Y.: Temporospatial variations and Spearman correlation analysis of ozone concentrations to nitrogen dioxide, sulfur dioxide, particulate matters and carbon monoxide in ambient air, China, Atmospheric Pollution Research, 10, 1203-1210, https://doi.org/10.1016/j.apr.2019.02.003, 2019b.

Witte, J., Duncan, B., Douglass, A., Kurosu, T., Chance, K., and Retscher, C.: The unique OMI HCHO/NO_2 feature during the 2008 Beijing Olympics: Implications for ozone production sensitivity, 45, 3103-3111, 2011.

Xing, J., Wang, S. X., Jang, C., Zhu, Y., and Hao, J. M.: Nonlinear response of ozone to precursor emission changes in China: a modeling study using response surface methodology, Atmos. Chem. Phys., 11, 5027-5044, 10.5194/acp-11-5027-2011, 2011.

Xing, J., Li, S., Jiang, Y., Wang, S., Ding, D., Dong, Z., Zhu, Y., and Hao, J.: Quantifying the emission changes and associated air quality impacts during the COVID-19 pandemic on the North China Plain: a response modeling study, Atmos. Chem. Phys., 20, 14347–14359, https://doi.org/10.5194/acp-20-14347-2020, 2020.

Xue, L. K., Wang, T., Gao, J., Ding, A. J., Zhou, X. H., Blake, D. R., Wang, X. F., Saunders, S. M., Fan, S. J., Zuo, H. C., Zhang, Q. Z., and Wang, W. X.: Ground-level ozone in four Chinese cities: precursors, regional transport and heterogeneous processes, Atmos. Chem. Phys., 14, 13175-13188, 10.5194/acp-14-13175-2014, 2014.

Zara, M., Boersma, K. F., De Smedt, I., Richter, A., Peters, E., van Geffen, J. H. G. M., Beirle, S., Wagner, T., Van Roozendael, M., Marchenko, S., Lamsal, L. N., and Eskes, H. J.: Improved slant column density retrieval of nitrogen dioxide and formaldehyde for OMI and GOME-2A from QA4ECV: intercomparison, uncertainty characterisation, and trends, Atmos. Meas. Tech., 11, 4033-4058, 10.5194/amt-11-4033-2018, 2018.

Zeng, Y., Cao, Y., Qiao, X., Seyler, B. C., and Tang, Y.: Air pollution reduction in China: Recent success but great challenge for the future, Science of the Total Environment, 663, 329-337, 2019.

Zhang, H., Wang, S., Hao, J., Wang, X., Wang, S., Chai, F., and Li, M.: Air pollution and control action in Beijing, Journal of Cleaner Production, 112, 1519-1527, https://doi.org/10.1016/j.jclepro.2015.04.092, 2016.

Zhao, Y., Zhang, K., Xu, X., Shen, H., Zhu, X., Zhang, Y., Hu, Y., and Shen, G.: Substantial Changes in Nitrogen Dioxide and Ozone after Excluding Meteorological Impacts during the COVID-19 Outbreak in Mainland China, Environmental Science & Technology Letters, 7, 402-408, 10.1021/acs.estlett.0c00304, 2020.

Zoran, M. A., Savastru, R. S., Savastru, D. M., and Tautan, M. N.: Assessing the relationship between ground levels of ozone (O_3) and nitrogen dioxide (NO_2) with coronavirus (COVID-19) in Milan, Italy, Science of The Total Environment, 740, 140005, https://doi.org/10.1016/j.scitotenv.2020.140005, 2020.

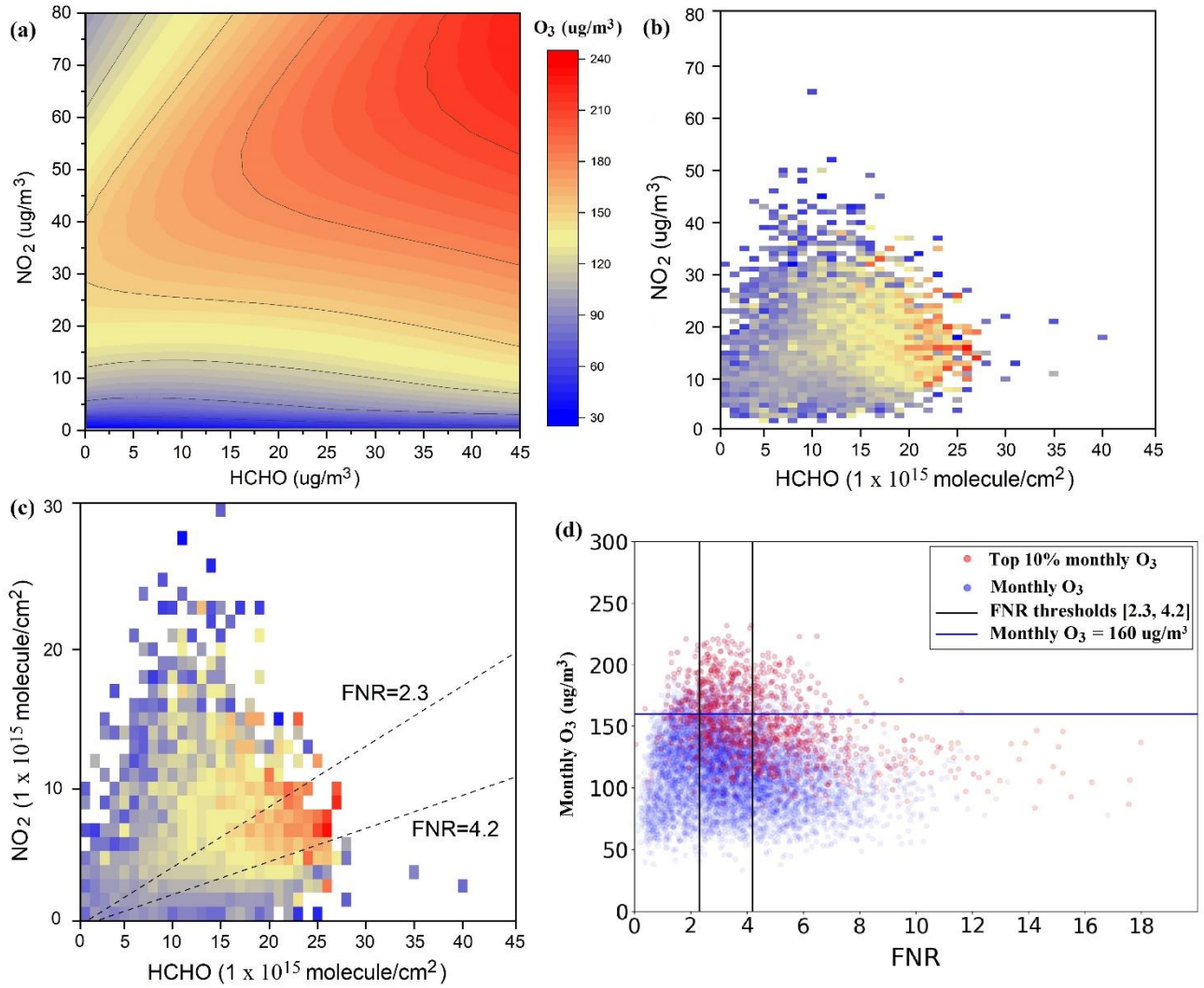

Figure 1: (a) The simulated O_3 isopleths versus NO_2 and HCHO using the CLASS model. (b) The 360 cities' monthly mean *in-situ* O_3 concentrations versus *in-situ* NO_2 concentrations and HCHO columns from OMI observations in the summer during 2016-2019. Note: daily ground-based O_3 and NO_2 observations are calculated from hourly observations at OMI overpass time (averaged at 13:00 LT and 14:00 LT). The O_3 numeric value of the grid cells is average of all points falling in each bin. (c) same as (b), but with NO_2 columns from OMI observations. (d) The top 10% monthly O_3 values and corresponding FNRs of each city. FNR thresholds are defined as the ±30% range from the median of monthly O_3 exceeding 160 µg/m^3 in the top 10% dataset.

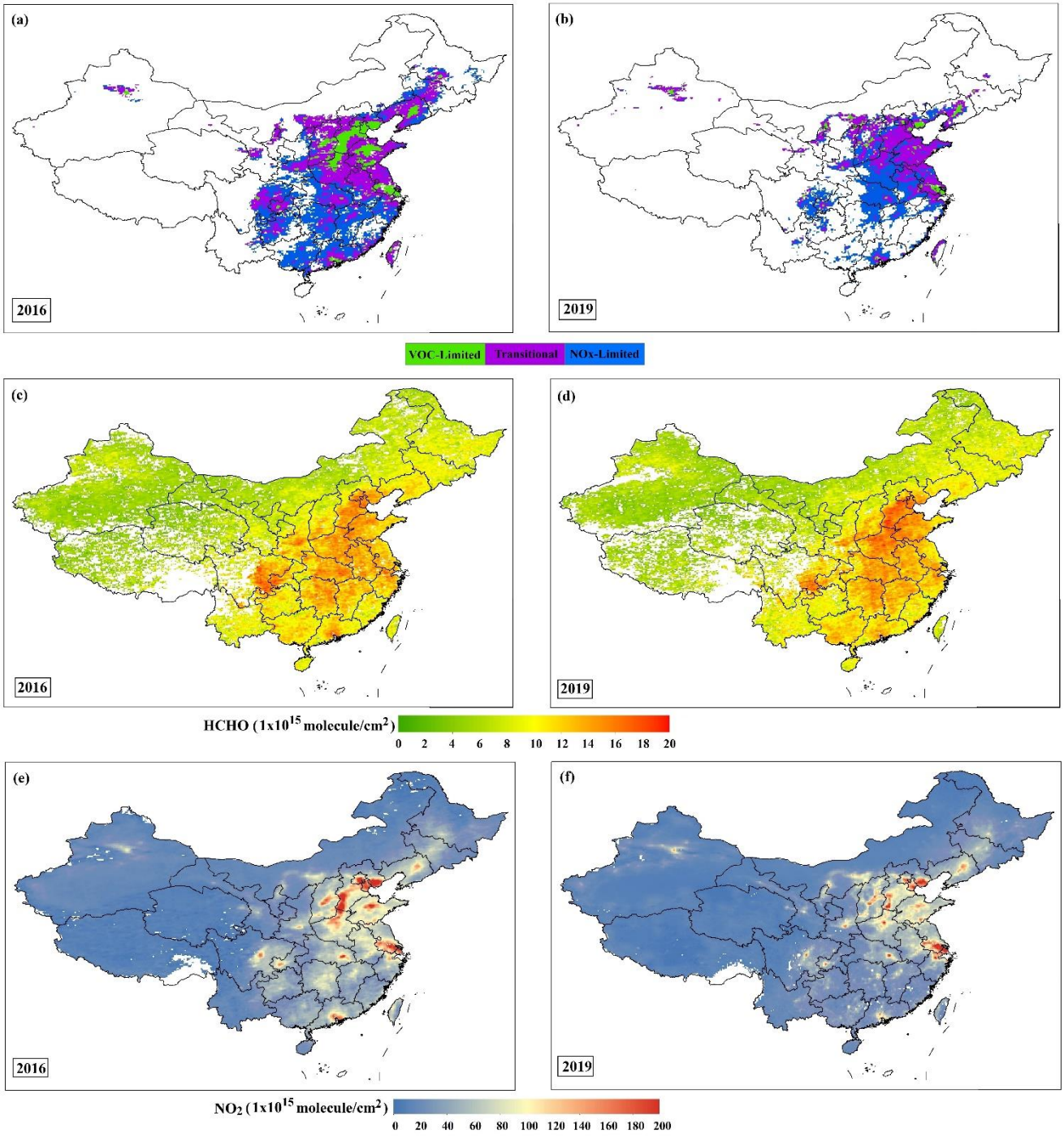

Figure 2: (a) Photochemical regime classification over China in the summer of 2016. (b) Same as (a), but for 2019. Note: no data grids in (a) and (b) corresponds to monthly HCHO columns below the detection limit (2×10^{15} molecule/cm^2) or NO_2 columns lower than 1.5×10^{15} molecule/cm^2. (c) Mean HCHO columns from OMI over China in the summer of 2016. (d) Same as (c), but for 2019. (e) Mean NO_2 columns from OMI over China in the summer of 2016. (f) Same as (e), but for 2019.

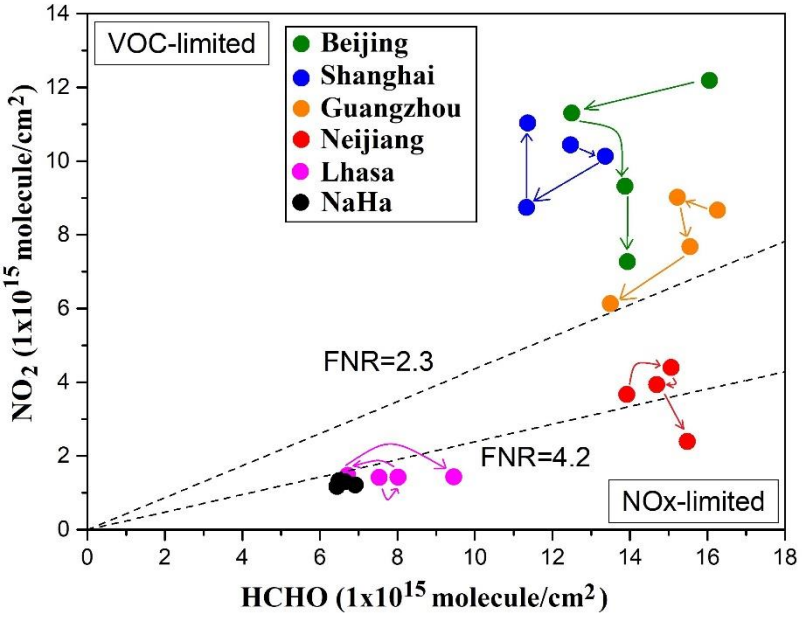

Figure 3: The change of O_3 formation sensitivity of six cities (Beijing, Shanghai, Guangzhou, Neijiang, Lhasa and NaHa) in summer from 2016 to 2019. The arrows represent time step from 2016 to 2019.

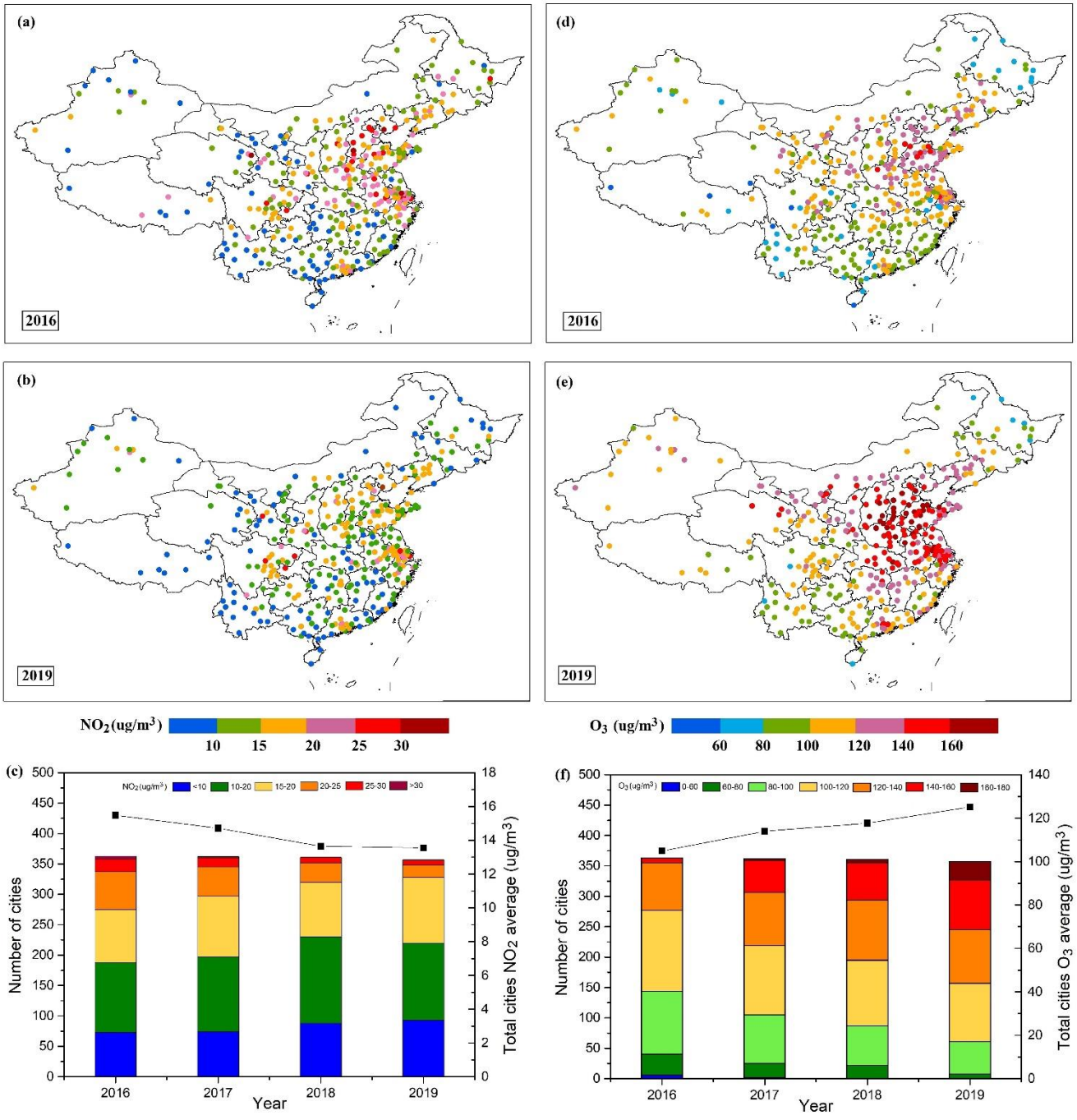

Figure 4: (a) Mean ground-based NO_2 concentration at each city in the summer of 2016. (b) Same as (a) but for 2019. (c) The bars indicate the number of cities (left axis) in a certain NO_2 range in summer from 2016 to 2019. The black line indicates the average NO_2 concentration (right axis) of all cities. (d) Mean ground-based O_3 concentration at each city in summer of 2016. (e) Same as (d) but for 2019. (f) Same as (c) but for O_3. Note: daily *in-situ* NO_2 and O_3 data is the average of 13:00-14:00 of the sites in each city.

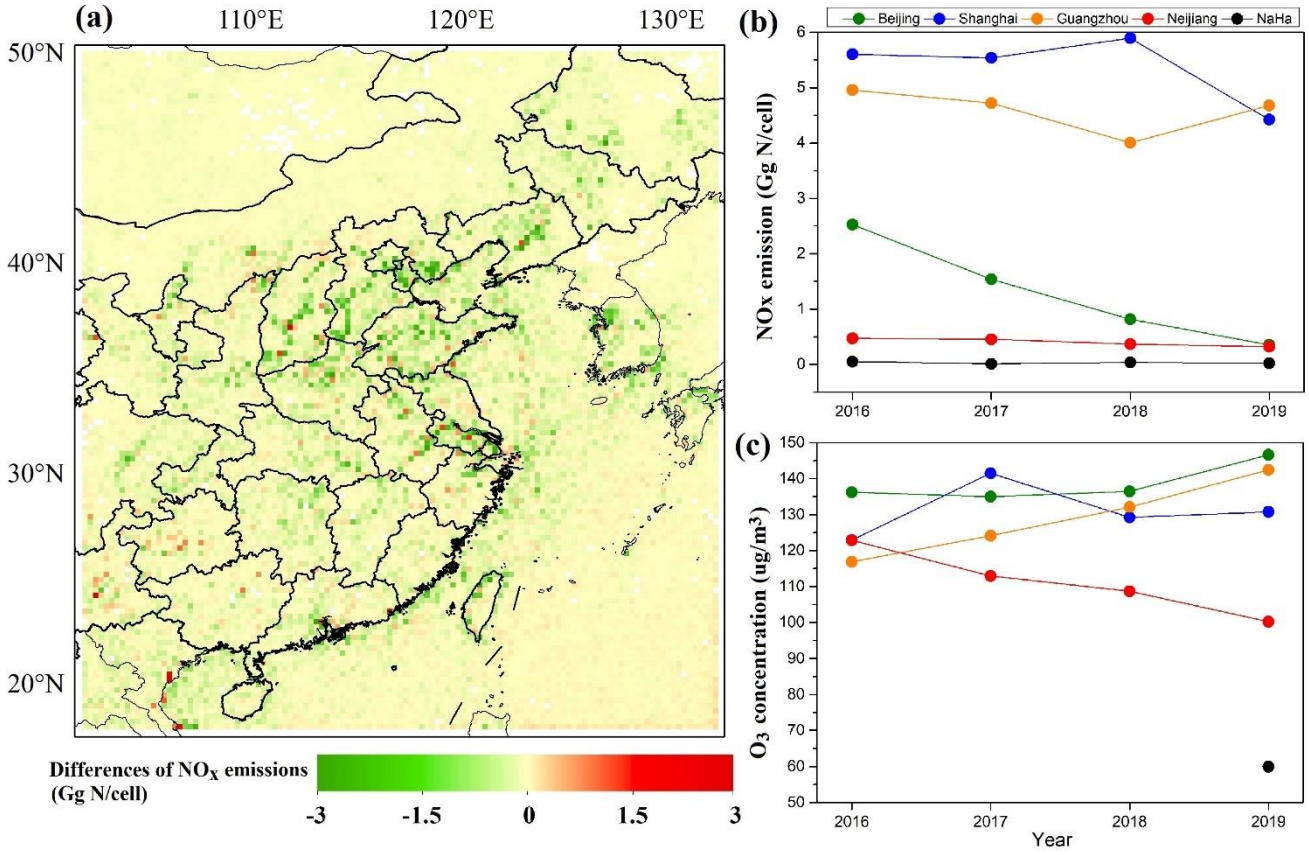

Figure 5: (a) Differences of total NO_x emissions derived from OMI observations in summer in east China between 2019 and 2016. (b) Variations of total NO_x emissions in five cities (Beijing, Shanghai, Guangzhou, Neijiang and NaHa) in summer from 2016 to 2019. (c) Variations of mean ground-based O_3 concentrations in five cities in summer from 2016 to 2019.

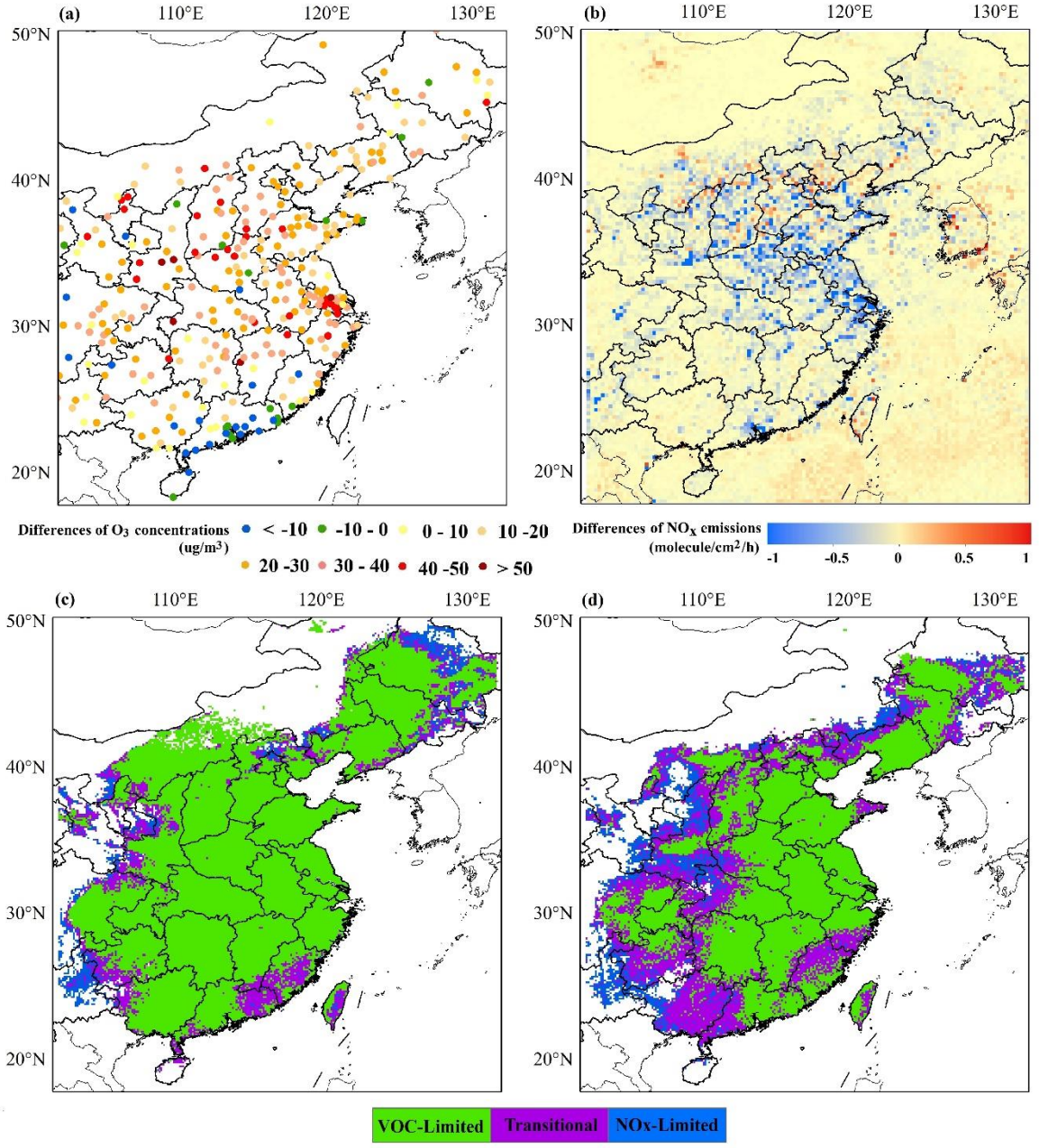

695

Figure 6: (a) Differences of mean ground-based O_3 concentrations in east China between period I and period II. (b) Differences of mean NO_x emissions in east China between period I and period II. (c) O_3 formation sensitivity in east China during period I. (d) Same as (c), but for period II. Note: Period I (3 - 23 January, 2020) is before the lockdown and period II (9 - 29 February, 2020) is during the lockdown.